Sediment Processes and Flow Reversal in the Undular Tidal Bore of the Garonne River

D. Reungoat, Hubert Chanson, Bastien Caplain

Sediment Processes and Flow Reversal in the Undular Tidal Bore of the Garonne River

by

David Reungoat ([1]), Hubert Chanson ([2]),and Bastien Caplain ([1])

([1]) Université de Bordeaux, I2M, 16 avenue Pey-Berland, Pessac, France, CNRS UMR 5295, Pessac, France

([2]) The University of Queensland, School of Civil Engineering, Brisbane QLD 4072, Australia

Corresponding author, Email: h.chanson@uq.edu.au, Ph.: (61 7) 3365 3619, Fax: (61 7) 3365 4599, Url: http://www.uq.edu.au/~e2hchans/

Abstract

A tidal bore is a series of waves propagating upstream as the tidal flow turns to rising, and the bore front corresponds to the leading edge of the tidal wave in a funnel shaped estuarine zone with macro-tidal conditions. Some field observations were conducted in the tidal bore of the Garonne River on 7 June 2012 in the Arcins channel, a few weeks after a major flood. Despite the high initial water level and strong fluvial current, the bore front exhibited a sharp discontinuity in terms of free-surface elevation: the bore front was 0.45 m and 0.52 m high on the morning and afternoon respectively. The tidal bore was a flat undular bore with a Froude number close to unity: Fr_1 = 1.02 and 1.19 in the morning and afternoon respectively. The field observations highlighted a number of unusual features on the morning of 7 June 2012 when detailed free-surface and velocity measurements were conducted simultaneously. These included (a) a slight rise in water elevation starting about 70 s prior to the front, (b) a flow reversal about 50 s after the bore front, (c) some large fluctuations in suspended sediment concentration (SSC) about 100 s after the bore front and (d) a transient water elevation lowering about 10 minutes after the bore front passage. The measurements of water temperature and salinity showed nearly identical results before and after the tidal bore: there was no evidence of saline or thermal front.

Keywords: Undular tidal bore, Garonne River, Suspended sediment processes, Flow reversal, Field measurements.

1. INTRODUCTION

A tidal bore is a series of waves propagating upstream as the tidal flow turns to rising, and the bore front corresponds to the leading edge of the tidal wave in a funnel shaped estuarine zone with macro-tidal conditions. Technically the tidal bore is a positive surge associated with a sudden rise in water depth and a discontinuity of the velocity and pressure fields The strength is the bore is often expressed in terms of its Froude number (TRICKER 1965, LIGHTHILL 1978). When the Froude number is between unity and 1.4 to 1.7, the bore front is followed by a train of well-defined secondary waves called whelps. Figure 1 illustrates some undular tidal bore in the Garonne River. For large Froude numbers, a breaking bore is observed. A tidal bore may have a variety of different shapes (TRICKER 1965, CHANSON 2011), and the photographic observations illustrated in particular that the bore front is not a sharp, vertical discontinuity of the water surface because of the necessary curvature of the streamline and the associated pressure and velocity redistributions. It is estimated worldwide that over 400 estuaries and shallow-water bays are affected by a tidal bore process (BARTSCH-WINKLER and LYNCH 1988, CHANSON 2011).

A number of field studies experienced some damage to scientific equipments, including in the Rio Mearim (Brazil), in the Daly River (Australia), in the Dee River (UK) and in the Bay of Mont Saint Michel (France) (KJERFVE and FERREIRA 1993, WOLANSKI et al. 2004, SIMPSON et al. 2004, MOUAZE et al. 2010). These incidents highlighted the intense turbulent mixing induced by the bore. Further field studies demonstrated the impact of the bore on sediment processes (CHEN et al. 1990, TESSIER and TERWINDT 1994, GREB and ARCHER 2007, CHANSON et al. 2011). During the 13th century, CHIEN Yueh-yu observed the Qiantang River bore (China) with insights: "*the turbid waters are piled up and the water behind comes on in a mass, and then it busts over the sand-flats with fury and boiling rage and tremendous sound*" (MOULE 1923). Altogether past observations and field studies demonstrated that the arrival of the bore front was associated with intense bed material mixing and upstream advection of suspended sediments behind the bore.

Some field measurements were conducted in the Garonne River (France) on 7 June 2012. The present study was conducted at the same site as CHANSON et al. (2011), but a few weeks after a major flood in April-May. The water level was higher in 2012 and the river bed might have been scoured from the soft sediments during the flood. Some turbulent velocity measurements were performed continuously at high-frequency (50 Hz) in the undular bore. Despite a number of practical issues and problems, the results provided a detailed characterisation of the unsteady flow features and sediment processes in the tidal bore, including some unusual flow reversal.

2. MATERIALS AND METHODS

2.1 Presentation

The Gironde estuary extends for about 72 km from the Pointe de Grave to Bec d'Ambès at the confluence of the Garonne and Dordogne Rivers, and it is navigable for oceangoing vessels up to Bordeaux, despite sandbanks and strong tides. Its funnel shape and bathymetry amplifies the tidal range. For example, when the tidal range is 4.5 m at Pointe de Grave, at the mouth of Gironde, the tidal range at Bordeaux is 5.5 m (Predicted tidal ranges on 7 June 2012). The Garonne River is 575 km long plus the Gironde Estuary and its intertidal zone extends up to Castets. The catchment area is 56,000 km^2. The tidal bore is observed typically from Pont François Mitterand (Bordeaux) up to Cadillac. The field study was conducted in the Garonne River (France) in the *Bras d'Arcins* (Arcins channel) between *Île d'Arcins* (Arcins Island) and the right bank close to Lastrene (Fig. 1). The location (44°47'58"N, 0°31'07"W) is seen in Figure 2A. The Arcins channel is about 1.8 km long, 70 m wide and about 1.1 to 2.5 m deep at low tide. Figure 3A presents a cross-sectional survey conducted on 7 June 2012, and the data are compared with the bathymetric survey conducted at the same location on 10 September 2010 with z being the vertical elevation. The comparison higlihgted a slightly deeper bed and higher initial water level during the 2012 study (Fig. 3A). In Figure 3B, the details of the velocimeter location are shown. Figure 3C presents the water elevation observations at Bordeaux and the water elevations recorded on-site prior to and shortly after the passage of the tidal bore on 7 June 2012. All the water elevations are given in m NGF IGN69. Although the tides are semi-diurnal, the tidal cycles have slightly different periods and amplitudes indicating some diurnal inequality (Fig. 3C).

The field measurements were conducted under spring tide conditions on 7 June 2012 morning and evening. The tidal range data are summarised in Table 1 (column 3). During the study, the water elevations and some continuous high-frequency turbulence data were recorded prior to, during and after the passage of the tidal bore for a few hours in the morning. The start and end times are listed in Table 1. No ADV recording was conducted during the afternoon bore because of damage to the ADV unit (see below). Further details were reported in REUNGOAT et al. (2012).

2.2 Instrumentation

The free surface elevations were measured manually using a survey staff. During the passage of the tidal bore, a video camera recorded the water level and the data were collected at 50 frames per seconds (fps). The survey staff was mounted 2 m beside the ADV unit towards the right bank, to minimise any interference with the ADV sampling volume. The water temperature and salinity were measured with an alcohol thermometer and salinity meter Ebro

Electronic SSX56 respectively. The readings were taken about 0.5 m (morning) to 1 m (afternoon) below the free-surface.

During the morning bore, the turbulent velocities were measured with a Sontek™ microADV (16 MHz, serial number A1036F). The ADV system was equipped with a 3D side-looking head. The system was fixed at the downstream end of a 23.55 m long heavy, sturdy pontoon. It was mounted vertically, the emitter facing towards Arcins Island, and the positive direction head was pointing downstream. Figure 3B shows the location of the ADV sampling volume in the surveyed cross-section. The sampling volume was about 1.03 m below the free-surface (Table 1, column 10 & Fig. 3B). All the ADV data underwent a post-processing procedure to eliminate any erroneous or corrupted data from the data sets to be analysed. The post processing was conducted with the software WinADV™ version 2.028, including the removal of communication errors, the removal of average signal to noise ratio (SNR) data less than 15 dB and the removal of average correlation values less than 60% (McLELLAND and NICHOLAS 2000). Further observations were recorded with digital cameras Pentax™ K-7, Pentax™ K-01, Sony™ Alpha 33 (30 fps), and a HD digital video camera Canon™ HF10E (50 fps).

Some Garonne River bed material was collected at low tide on 7 June 2012 afternoon, and at mid-ebb tide on 8 June 2012 afternoon next to the pontoon on the right bank at Arcins. The soil sample consisted of fine mud and silt materials collected on the stream bed just above the free-surface water mark. A series of laboratory tests were conducted to characterise the bed material. The soil sample granulometry was measured with a Malvern™ laser Mastersizer 2000 equipped with a Hydro 3000SM dispersion unit for wet samples. For each sediment sample, two mixing techniques were tested: mechanical and ultrasound, for durations ranging from 10 to 30 minutes. For a given configuration, the granulometry was performed four times and the results were averaged. The differences between the 4 runs were checked and found to be negligible. The rheological properties of mud samples were tested with a rheometer Malvern™ Kinexus Pro (Serial MAL1031375) equipped with either a plane-cone (∅ = 40 mm, cone angle: 4°) or a plane-disk (∅ = 20 mm). The gap truncation (150 μm) was selected to be more than 10 times the mean particle size. The tests were performed under controlled strain rate at constant temperature (25 Celsius). Between the sample collection and the tests, the mud was left to consolidate for 5 days. Prior to each rheological test, a small mud sample was placed carefully between the plate and cone. The specimen was then subjected to a controlled strain rate loading and unloading between 0.01 s^{-1} and 1,000 s^{-1} with a continuous ramp.

The acoustic backscatter properties of the ADV unit were calibrated by measuring the signal amplitude of known, artificially produced concentrations of material obtained from the bed material sample, diluted in tap water and thoroughly mixed. All the experiments were conducted within 5 days of the field experiment. The laboratory

experiments were conducted with the same Sontek^{TM} microADV (16 MHz, serial A1036F) system using the same settings. For each test, a known mass of sediment was introduced in a water tank which was continuously stirred with a paint mixer. The mixer speed was adjusted during the most turbid water tests to prevent any obvious sediment deposition on the tank bottom. The mass of wet sediment was measured with a Mettler™ Type PM200 (Serial 86.1.06.627.9.2) balance. The mass concentration was deduced from the measured mass of wet sediment and the measured water tank volume. During the tests, the suspended sediment concentrations (SSCs) ranged from less than 0.01 kg/m^3 to 100 kg/m^3.

During the acoustic backscatter amplitude measurement, the ADV signal outputs were scanned at 50 Hz for 180 s for each test. The average amplitude measurements represented the average signal strength of the three ADV receivers. For low SSCs, the ADV data were post-processed with the removal of average signal to noise ratio data less than 15 dB, average correlation values less than 60%, and communication errors. For SSC > 60 kg/m^3, unfiltered data were used since both the SNRs and correlations dropped drastically because of signal attenuation.

2.3 Practical considerations

The accuracy on the ADV velocity measurements was 1% of the velocity range (± 2.5 m/s) (Sontek 2008). The accuracy of the water elevation was 0.5 cm prior to the tidal bore and 1-2 cm during the tidal bore passage. The mass of wet sediment was measured with an accuracy of less than 0.01 g, and the SSC was estimated with an accuracy of less than 0.001 g/l. The water elevation measurements and ADV data were synchronised within a second. All cameras and digital video cameras were also synchronised together with the same reference time within a second.

During the field deployment, a major problem was experienced: the ADV stem was bent along the main upstream flow direction by about 12° (REUNGOAT et al. 2012). The damage was noted when the unit was retrieved at the end of the study. Based upon the visual observations and ADV record, it is believed that the ADV unit stem was hit by a submerged debris during the early flood tide, about 1 h after the bore passage. After the ADV system was brought back in the laboratory, the unit was inspected and checked. While the outcomes were successful, the authors acknowledge that this physical damage might have some effect on the ADV data, in particular the vertical component. Further the suspended sediment tests were performed with the ADV unit four days later and the results indicated no apparent issue with the ADV operation. Nonetheless the velocity data set must be considered with care.

4. RESULTS

4.1 Basic observations

The tidal bore propagation in the Arcins channel (*Bras d'Arcins*) was studied on 7 June 2012 both morning and evening, after being observed on 4 and 5 June 2012 evenings (Fig. 1). The tidal bore formed first at the downstream end of the channel. The tidal bore extended across the entire channel width as an undular bore (Fig. 1A), even a very flat one as seen on 7 June 2012 morning (Fig. 1B). As the bore propagated upstream, its shape evolved constantly in response to the local bathymetry. The tidal bore was undular when it passed the sampling location. On 7 June afternoon, the bore front was well marked by some kayakers riding ahead of the first wave crest (Fig. 1C). The bore continued to propagate up to the upstream end of the channel for another few minutes, although it is conceivable that the tidal bore of the Garonne River main channel entered the southern end of the Arcins channel (Fig. 2B). The passage of the tidal bore was characterised by a pseudo-chaotic surface motion lasting for several minutes after the bore front. At the sampling location, the free-surface elevation rose very rapidly by 0.45 m and 0.52 m in the first 10-15 seconds on 7 June 2012 morning and afternoon respectively. On the 7 June 2012 morning, the bore front was barely perceptible, but the rapid rise in water elevation was thoroughly documented.

The tidal bore is a hydrodynamic shock which is characterised by its Froude number defined as (HENDERSON 1966, CHANSON 2012):

$$Fr_1 = \frac{U + V_1}{\sqrt{g \times \frac{A_1}{B_1}}} \quad (1)$$

where V_1 is the river flow velocity prior to the bore, U is the bore celerity for an observer standing on the bank, g is the gravity acceleration, and A_1 and B_1 are respectively the channel cross-sectional area and free-surface width prior to the bore. During the present field experiments, the tidal bore was undular and the tidal Froude number was estimated from the surveyed channel cross-section, water level observations and tidal bore celerity observations (Table 1). The tidal bore Froude number was Fr_1 = 1.02 and 1.19 for the field observations on 7 June 2012 morning and afternoon respectively.

The time-variations of water depth were recorded using a survey staff placed about 1.4 m beside the ADV towards the right bank. Figures 4A and 5A present the observations on 7 June 2012 morning and afternoon respectively. The water depth data showed qualitatively some similar trend. The water depth decreased slowly at the end of ebb tide prior to the tidal bore arrival. The passage of the bore was associated with a very rapid rise of the water elevation (t = 24,180 s & 67,620 s in Fig. 4A & 5A) and some pseudo-chaotic wave motion shortly after the front. During the following flood

flow, the water depth increased rapidly with time: i.e., nearly 1.4 and 1.8 m in 30 minutes on 7 June 2012 morning and afternoon respectively. Such features were previously seen in field experiments of undular tidal bores (WOLANSKI et al. 2004, CHANSON et al. 2011). There were however some unusual features observed herein. These included (a) a slow rise of water level immediately prior to the bore front on 7 June 2012 morning and (b) some unexpected water level drop about 10 minutes after the front. On 7 June 2012 morning, the free-surface depth data highlighted a gradual rise in water level immediately prior to the bore front: that is, a gentle rise of 0.04 m in about 70 s immediately prior to the front discontinuity for 24,110 < t < 24,180 s (Fig. 6). This is illustrated in Figure 6. Although some laboratory experiments reported a gentle rise in water level ahead of breaking bores (KOCH and CHANSON 2009, DOCHERTY and CHANSON 2012, KHEZRI and CHANSON 2012), the present observations might reflect the very flat nature of the tidal bore associated with the bore Froude number ($Fr_1 \approx 1.02$) close to unity. On both morning and afternoon of 7 June 2012, the authors were surprised by a rapid drop in water elevation of 0.1 m about 10 minutes after the passage of the bore front. This feature is highlighted in Figures 4A and 5B with a black arrow. No physical explanation can be proposed definitely, but it might be conceivable that the sudden water level drop, 10 minutes after the main bore front, was caused by the tidal bore of the main Garonne River channel entering into the southern end of the Arcins channel and propagating northwards against the flood flow (Fig. 2B). The situation is sketched in Figure 2B. Such a backward bore was previously seen at the southern end of the Arcins channel during previous tidal bore events and it occurs because the tidal bore front travels faster in the deeper waters of the Garonne River main channel. A similar phenomenon was observed in the River Trent (UK) (JONES 2012, *Pers. Comm.*).

The time-variations of water temperature and salinity data are presented in Figures 4B and 5B. The water temperature varied from 20 to 21 Celsius in the morning of 7 June 2012 and between 18 and 21 Celsius in the afternoon. The salinity of water ranged from 0.055 to 0.08 kg/m^3, or 55 to 80 ppm. These salinity values corresponded mostly to freshwater and the finding was consistent with the observations of the individuals who were in the water installing and dismantling the setup. The result implied that the effects of the recent (April-May 2012) flood of the Garonne River were still felt at the sampling site on 7 June 2012, while the present observations did not show any evidence of saline front nor temperature front on both morning and evening tidal bores on 7 June 2012. While some salinity and temperature fronts were sometimes reported behind tidal bores (review in CHANSON 2011, pp. 118-120), the present findings were collected at a sampling site located about 100 km from the river mouth (Pointe de Grave). It is likely that the upstream location together with the relatively large freshwater runoff prevented the occurrence of any salinity and temperature front.

4.2 Velocity measurements

On 7 June 2012 morning, the instantaneous velocity data showed the drastic impact of the tidal bore propagation. Figure 4C presents the time-variations of the velocity components and Figure 6 shows some detailed data about the bore passage, with the longitudinal velocity component V_x positive downstream towards Bordeaux, the transverse velocity component V_y positive towards the Arcins Island, and the vertical velocity component V_z positive upwards. The time-variations of the surface velocity data are included in Figure 4A. They were recorded in the middle of the Arcins channel using floating debris and carefully measured with stopwatches. The surface velocity observations highlighted the sudden flow reversal associated with the passage of the tidal bore. However, next to the ADV, the video observations indicated that the surface flow direction reversed about 6 s after the bore front on 7 June 2012 morning.

The ADV velocity data showed the marked effect of the passage of the bore front at t = 24,180 s despite the small bore height (Fig. 4C & 6). The longitudinal velocity component data showed some rapid flow deceleration associated with the passage of the bore front although with some delay. The surface velocity data exhibited a similar general pattern, but the surface velocity magnitude was consistently larger than the longitudinal velocity magnitude recorded by the ADV. The ADV sampling volume was only 7 m from the river bank water line at low tide, and the slower ADV data might reflect the effect of river bank proximity.

The tidal bore passage was observed about t ≈ 24,180 s with the sudden rise in free-surface elevation. A time delay between the bore front passage and the longitudinal flow reversal was observed: this is highlighted in Figure 6. That is, the data showed the reversal in longitudinal flow direction about 50 s after the bore front: i.e., t ≈ 24,330 s (Fig. 6). This unusual flow reversal differed from a number earlier observations including WOLANSKI et al. (2004), SIMPSON et al. (2004), CHANSON et al. (2011) and MOUAZE et al. (2010) in the field, and HORNUNG et al. (1995), KOCH and CHANSON (2009), CHANSON (2010) and DOCHERTY and CHANSON (2012) in laboratory. All these studies showed the flow reversal at the same time as the bore passage. However a few field studies reported some usual delay between the bore front arrival and the flow reversal (Table 2). These are summarised in Table 2 together with the present observations. Some observations reported a delay between bore passage and velocity reversal, while a study indicated an early flow reversal in the Rio Mearim (Brazil) (Table 2). In the Severn River (UK), ROWBOTHAM (1983) observed some delayed flow reversal depending upon the relative water elevation and bore strength. Although the authors do not have a definite explanation for the flow reversal delay, it is conceivable that the significant freshwater flow prior to the bore arrival tended to delay the reversal of flow at the ADV control volume. It is also possible that some flow stratification might have impacted the velocity field with the denser saltwater close to the channel bed, although no vertical distribution of salinity was measured.

The tidal bore passage was characterised by some large fluctuations of all three velocity components. The longitudinal flow component changed from +0.4 m/s oriented downriver to -0.65 m/s oriented upriver immediately after the passage of the bore, with turbulent fluctuations between 0 to -1 m/s. The large velocity fluctuations lasted for the entire sampling duration (Fig. 4C). The longitudinal velocity results were consistent with the free-surface velocity observations before and after the tidal bore passage, although the surface current was stronger on the channel centreline. After the passage of the bore, the transverse velocities fluctuated between -0.25 and +0.55 m/s, and the time-averaged transverse velocity component was +0.16 m/s (Fig. 4C). The finding implied some net transverse circulation towards the left bank at 1.03 m beneath the free-surface. This flow pattern was possibly linked with the irregular channel cross-section and the existence of some secondary flow motion. The vertical velocity data highlighted a marked effect of the tidal bore. After the bore passage, the vertical velocity fluctuated between -0.1 and +1.3 m/s, with a time-averaged value of about -0.08 m/s.

Overall the bore arrival of the bore was characterised with a rapid rise of the water elevation associated with a delayed flow deceleration. The flow reversal process lasted about 5-7 s, compared to about 10 s for the bore front passage. The sudden flow deceleration, of magnitude 0.107 m/s^2, was followed with large and rapid fluctuations of all three velocity components. These large and rapid fluctuations lasted several minutes after the bore passage (Fig. 4C & 6). The longitudinal velocity data presented some long-period fluctuations with periods of about 40 s (Fig. 4C) starting after the flow reversal. These might be caused by some form of seiche which was possibly linked with some transverse sloshing in the Arcins channel. Lastly note that the ADV sampling volume depth was about 1.03 m for the entire study duration. That is, the velocity data characterised the turbulence in the upper water column. The ADV unit was fixed to a pontoon, whose vertical motion of the pontoon cannot be ignored.

4.3 Sediment properties

The bed sediment material was characterised by a series of laboratory experiments. The relative density of the wet sediment samples was about **s** = 1.36 to 1.48. Assuming a relative sediment density of 2.65, this corresponded to a sample porosity of 0.70 to 0.78. The particle size distribution data presented close results for all samples although they were collected over two different days at different locations. The median particle size was basically 13 μm (Φ = 6.3) corresponding to some silty materials (GRAF 1971, JULIEN 1995, CHANSON 2004). The sorting coefficient $\sqrt{d_{90} / d_{10}}$ ranged from 3.3 to 4.2. The bed material was basically a cohesive mud mixture and the granulometry data were nearly independent of the sample and mixing technique.

The rheometry tests provided some information on the relationship between shear stress and shear rate during the loading and unloading of small sediment quantities. A range of tests were performed with two configurations, and two sediment samples for each configuration. The sediment sample collected on 7 June 2012 appeared to be more cohesive and less homogeneous: e.g., the authors found some darker sediment inclusions as well as some fibres. The relationship between shear stress and shear rate highlighted some basic differences between the loading and unloading phases typical of some form of material thixotropy. The magnitude of the shear stress during unloading was smaller than the shear stress magnitude during loading for a given shear rate (Fig. 7). Figure 7 presents a typical example of rheometry data. The data were used to estimate an apparent yield stress of the fluid τ_c and effective viscosity μ. The former is related to the minimum boundary shear stress required to erode and re-suspend the sediments (OTSUBO and MURAOKO 1998). The yield stress and viscosity were estimated by fitting the rheometer data with a Herschel-Bulkley model, during the unloading phase to be consistent with earlier thixotropic experiments (ROUSSEL et al. 2004, CHANSON et al. 2006):

$$\tau = \tau_c + \mu \times \left(\frac{\partial V}{\partial y} \right)^m \quad (2)$$

with $0 < m \leq 1$. Based upon the unloading data, the data were consistent with the qualitative observations: that is, a more cohesive sediment mixture was collected on 7 June 2012 associated with larger yield stress and apparent viscosity. On average, the apparent viscosity was between 18 and 36 Pa.s, the yield stress was about 75 to 271 Pa and $m \sim 0.22$ and 0.40 for the sediment sample collected on 7 June 2012 at low tide. For the sediment sample collected on 8 June 2012 at mid-ebb tide, the apparent viscosity was between 2.9 and 13 Pa.s, the yield stress was about 15 to 74 Pa and $m \sim 0.27$ to 0.60 on average. The present results were comparable to the sediment properties of samples collected at Arcins on 11 September 2010, but it must be stressed that the present study was conducted shortly after a major flood of the Garonne River. An unique feature of the present data set was the range of rheometry data complemented by detailed granulometry tests, although with a limited protocol.

The relationship between the ADV acoustic backscatter amplitude (Ampl) and suspended sediment concentration (SSC) was tested systematically for SSCs between 0 and 100 kg/m^3. Two water solutions were used: de-ionised (permutted) water and tap water, and two sediment samples were tested: a sample collected at low tide on 7 June 2012 and another collected at mid-ebb tide on 8 June 2012. First the results were independent of the water solutions and sediment samples (Fig. 8). No difference was observed between the de-ionised (permutted) and tap water solutions, nor between the sediment samples collected at low tide on 7 June 2012 and mid-ebb tide on 8 June 2012. Second there was a good correlation between the results highlighting a characteristic relationship between SSC and amplitude. That is, a

monotonic increase in SSC with increasing backscatter amplitude for small SSCs, and a decreasing backscatter amplitude with increasing SSC for larger SSCs. The latter was linked with some ADV signal saturation as previously reported by HA et al. (2009), CHANSON et al. (2011) and BROWN and CHANSON (2013). For the laboratory tests with low suspended loads, the best fit relationships were:

$$\text{SSC} = \frac{-8.735}{1 - 35253 \times \exp(-0.1053 \times (\text{Ampl} - 92))} \qquad \text{SSC} \leq 8 \text{ kg/m}^3 \quad (3)$$

where the suspended sediment concentration SSC is in kg/m^3, and the amplitude Ampl is in counts. For large suspended sediment loads, the data were best correlated by

$$\text{SSC} = 240.34 - 1.582 \times \text{Ampl} + 0.00196 \times \text{Ampl}^2 \qquad \text{SSC} > 8 \text{ kg/m}^3 \quad (4)$$

Equations (3) and (4) are compared with the data in Figure 8.

In the Garonne River, CHANSON et al. (2011) measured SSC levels between 20 and 100 kg/m^3. In the North Branch of Changjiang estuary (China), CHEN (2003) measured surface water SSCs up to 16 kg/m^3 during the tidal bore. In the Qiantang River bore (China), SSC measurements of 20 to 50 kg/m^3 were reported (ZHOU and GAO 2004, ZHANG and LIU 2011). All these suggested that the SSCs were greater than 8 kg/m^3 in the Arcins channel bore on 7 June 2012, and Equation (4) was representative of the relationship between the suspended sediment concentration (SSC) and signal amplitude (Ampl).

4.4 Suspended sediment estimates

The time-variations of the suspended sediment concentration estimates are presented in Figure 4D for the field study on 7 June 2012 morning. The complete data set showed some nearly constant SSC (~ 34 kg/m^3 on average) at end of ebb tide prior to the tidal bore arrival (Fig. 4D). The passage of the tidal bore and ensuing flow reversal were associated with large fluctuations in SSC about 100 s after the bore passage. A similar unusual event was observed about 100 s after the tidal bore front during a previous study on 10 and 11 September 2010 in the Garonne River (CHANSON et al. 2011). For both studies (Table 1), the data indicated a significant decrease in SSC 100 s after the bore front passage (t = 24,300 s in Fig. 4D) followed by large and rapid fluctuations in SSCs: e.g., between t = 24,250 and 24,350 s in Figure 4D. During the flood flow, the SSC levels tended to decrease down to 26 kg/m^3 on average about 22 minutes (1350 s) after the bore passage. Afterwards the average SSC increased up to a level about 32 kg/m^3, comparable to that observed at the end of ebb tide. In addition, the authors observed visually some turbulent patches of muddy waters at the free-surface during the flood flow after the tidal bore. The free-surface waters appeared murkier than those at the end of ebb tide.

The velocity and SSC data were used to calculate the instantaneous suspended sediment flux per unit area q_s defined as:

$$q_s = SSC \times V_x \quad (5)$$

where q_s and V_x are positive in the downstream direction. In Equation (5), the SSC is in kg/m^3, the longitudinal velocity component V_x is in m/s and the sediment flux per unit area q_s is in kg/m^2/s. Herein q_s represents a sediment flux per unit area. The suspended sediment flux data showed typically a downstream positive suspended sediment flux during the end of the ebb tide prior to the tidal bore (Fig. 4D). On average, the suspended sediment flux per unit area was 14 kg/m^2/s prior to the bore. The arrival of the tidal bore was characterised by a rapid flow reversal and the suspended sediment flux was negative during the flood tide after the flow reversal. The instantaneous sediment flux data q_s showed some large and rapid time-fluctuations that derived from a combination of velocity and suspended sediment concentration fluctuations (Fig. 4). The high-frequency fluctuations in suspended sediment flux were likely linked with some sediment flux bursts caused by some turbulent bursting phenomena next to the channel boundaries. Some low-frequency fluctuations in sediment flux were also observed after the bore passage with a period of about 10 minutes (Fig. 4D).

5. DISCUSSION

For the present data set, the sediment flux data were integrated with respect of time to yield the net sediment mass transfer per unit area during a period T:

$$\int_T SSC \times V_x \times dt \quad (6)$$

Prior the tidal bore (22,125 < t < 24,340 s), the net sediment mass transfer per unit area was positive and Equation (6) yielded +28,040 kg/m^2 during the 37 minutes of ebb tide data prior the tidal bore. After the bore passage, the net sediment mass transfer per unit area was negative and equalled -201,650 kg/m^2 for 24,340 < t < 32,400 s (i.e. 136 minutes). That is, the net sediment flux was about two times larger in magnitude after the bore than the sediment flux prior to the tidal bore. The present findings may be compared with the results of CHANSON et al. (2011) in the Arcins channel on 11 September 2010 (Table 1). The 2010 study was conducted at the end of a dry summer, and the net suspended sediment flux per unit area was 8 times less prior to the bore than that observed in 2012. The difference was likely linked with the relatively stronger freshwater flow in June 2012. After the bore passage, the magnitude of suspended sediment flux per unit area was twice as large in 2010 as that in 2012. That is, the tidal bore re-mobilised a larger suspended sediment flux in September 2010. The difference might be the combined result of the slightly less

vigorous flood flow in June 2012 together with a lesser amount of available sediment materials, following some bed scour during the April-May 2012 floods of the Garonne River. A number of past studies highlighted that the tidal bore passage was linked with some intense sediment mixing and upstream advection of suspended matters (CHEN 2003, GREB and ARCHER 2007, CHANSON et al. 2011). The present data set supported the same trend (Fig. 4).

A basic feature of the present data set was the rapid fluctuations in suspended sediment flux during the tidal bore passage and flood flow. Some integral time scales were calculated over 1,000 s in terms of the longitudinal velocity, suspended sediment concentration and suspended sediment flux, immediately prior to the tidal bore (i.e. 23,130 < t < 24,130 s) and following the flow reversal (i.e. 24,250< t < 25,250 s) on 7 June 2012 morning. Herein the integral time scale of the longitudinal velocity, SSC and sediment flux, denoted T_{Vx}, T_{SSC} and T_{qs} respectively, are defined as:

$$T_{Vx} = \int_{0}^{\tau(R_{XX}=0)} R_{xx}(V_x(t), V_x(t+\tau)) \times d\tau \quad (7)$$

$$T_{SSC} = \int_{0}^{\tau(R_{XX}=0)} R_{xx}(SSC(t), SSC(t+\tau)) \times d\tau \quad (8)$$

$$T_{qs} = \int_{0}^{\tau(R_{XX}=0)} R_{xx}(q_s(t), q_s(t+\tau)) \times d\tau \quad (9)$$

where τ is the time lag and R_{xx} is the normalised auto-correlation function. The results showed some key differences between before and after the bore (Table 3). After the bore passage, the integral time scales were on average 20 times larger then those before the bore passage. The larger time scales may reflect the production of large eddies by the bore front and their upstream advection behind the bore, as hinted by some recent numerical modelling (LUBIN et al. 2010, FURUYAMA and CHANSON 2010). The comparison between turbulent and SSC integral time scales yielded a ratio of sediment to turbulence time scales $T_{SSC}/T_{Vx} \approx 0.1$, both before and after the bore. The result demonstrated some quantitative differences in timescales between the turbulent velocities and suspended sediment concentrations in a tidal bore flow, as discussed previously by CHANSON et al. (2007), TOORMAN (2008) and CHANSON and TREVETHAN (2011) in open channel and estuarine flows.

The physical data highlighted some significant sediment load with large SSCs and suspended sediment fluxes per unit area during the tidal bore event. Figure 9 shows the relationship between the average suspended sediment flux per unit area data as a function of the mean suspended sediment concentration after the tidal bore for the present study. The present data were compared with the 2010 study data and physical data recorded in rivers during floods and in estuaries (Fig. 9). The results (Fig. 9) demonstrate that high suspended sediment fluxes per unit area and SSC data were observed in the Garonne River tidal bore. While larger values were measured in some hyperconcentrated flow motion, the

present results showed higher suspended sediment concentrations and fluxes than in most rivers in flood.

6. CONCLUSION

Some field observations were conducted in the tidal bore of the Garonne River on 7 June 2012 in the Arcins channel, although the velocity measurements were conducted in the morning bore only because of some instrumentation damage. The present study was conducted at the same site as a series of field measurements performed in 2010 (CHANSON et al. 2011), but a few weeks after a major flood. The water level was higher in 2012 and the river bed might have been scoured from the soft sediments during the April-May 2012 flood. In 2012, the sediment bed material was cohesive with a median particle size of about 13 μm, and the mud exhibited a non-Newtonian behaviour. Some experiments under controlled conditions were performed to use the acoustic backscatter amplitude of the ADV as a surrogate estimate of the suspended sediment concentration (SSC).

On 7 June 2012, the tidal bore was a flat undular bore with a Froude number close to unity: Fr_1 = 1.02 and 1.19 in the morning and afternoon respectively. A feature of the study was some effect of recent floods (April-May 2012) of the Garonne River. At the end of ebb tide, the current was strong, the water level was relatively high and the water was predominantly some freshwater. Despite the high initial water level and strong fluvial current, the bore front exhibited a sharp discontinuity in terms of free-surface elevation: the bore front was 0.45 m and 0.52 m high on the morning and afternoon respectively. The field observations highlighted a number of unusual features on the morning of 7 June 2012. These included (a) a slight rise in water elevation starting about 70 s prior to the front, (b) a flow reversal about 50 s after the bore front, (c) some large fluctuations in suspended sediment concentration (SSC) about 100 s after the bore front and (d) a transient water elevation lowering about 10 minutes after the bore front passage. The measurements of water temperature and salinity showed nearly identical results before and after the tidal bore: there was no evidence of saline or thermal front.

The turbulent velocity data showed a marked impact of the tidal bore. The suspended sediment concentration (SSC) data indicated sediment concentrations between 20 and 40 kg/m^3 typically. Some large fluctuations in suspended sediment concentrations were observed about 100 s after the bore front, while some lower SSC levels were seen about 22 minutes after the tidal bore, before the SSC levels increased up to levels comparable to those before the bore. The data set yielded some substantial suspended sediment flux amplitudes consistent with the murky appearance of waters. After the passage of the bore, the net sediment mass transfer per unit area was negative (i.e. upriver) and its magnitude was twice as large as the net flux at the end of the ebb tide.

The present field data set presented a number of striking features rarely documented to date, including a delayed flow reversal and a transient water elevation lowering. These might be linked with the bore Froude number close to unity and the effects of a recent flood. On the other hand, the data highlighted a number of flow features previously documented in the field, including the large and rapid fluctuations in velocities and suspended sediment flux during the tidal bore. Importantly the present velocity record was a point measurement located 1.03 m beneath the free-surface, and any extrapolation to the entire channel cross-section would be inappropriate.

7. ACKNOWLEDGMENTS

The authors thank all the people who participated to the field works, without whom the study could not have been conducted. The authors acknowledge the assistance of Patrice BENGHIATI and the permission to access and use the pontoon in the *Bras d'Arcins*. The ADV was provided kindly by Prof Laurent DAVID (University of Poitiers, France). The financial assistance of the Agence Nationale de la Recherche (Projet MASCARET 10-BLAN-0911-01) is acknowledged, as well as the generous support of the project leader Dr Pierre LUBIN (University of Bordeaux, France).

8. REFERENCES

BARTSCH-WINKLER, S., and LYNCH, D.K. (1988). "Catalog of Worldwide Tidal Bore Occurrences and Characteristics." *US Geological Survey Circular*, No. 1022, 17 pages.

BAZIN, H. (1865). "Recherches Expérimentales sur la Propagation des Ondes." *Mémoires présentés par divers savants à l'Académie des Sciences*, Paris, France, Vol. 19, pp. 495-644 (in French).

BROWN, R., and CHANSON, H. (2013). "Suspended Sediment Properties and Suspended Sediment Flux Estimates in an Urban Environment during a Major Flood." *Water Resources Research*, AGU (DOI: 10.1029/2012WR012381). (in Print)

CHANSON, H. (2004). "The Hydraulics of Open Channel Flow: An Introduction." *Butterworth-Heinemann*, 2nd edition, Oxford, UK, 630 pages (ISBN 978 0 7506 5978 9).

CHANSON, H. (2010). "Unsteady Turbulence in Tidal Bores: Effects of Bed Roughness." *Journal of Waterway, Port, Coastal, and Ocean Engineering*, ASCE, Vol. 136, No. 5, pp. 247-256 (DOI: 10.1061/(ASCE)WW.1943-5460.0000048).

CHANSON, H. (2011). "Tidal Bores, Aegir, Eagre, Mascaret, Pororoca: Theory and Observations." *World Scientific*, Singapore, 220 pages (ISBN 9789814335416).

CHANSON, H. (2012). "Momentum Considerations in Hydraulic Jumps and Bores." *Journal of Irrigation and Drainage Engineering*, ASCE, Vol. 138, No. 4, pp. 382-385 (DOI 10.1061/(ASCE)IR.1943-4774.0000409).

CHANSON, H., JARNY, S., and COUSSOT, P. (2006). "Dam Break Wave of Thixotropic Fluid." *Journal of Hydraulic Engineering*, ASCE, Vol. 132, No. 3, pp. 280-293 (DOI: 10.1061/(ASCE)0733-9429(2006)132:3(280)).

CHANSON, H., REUNGOAT, D., SIMON, B., and LUBIN, P. (2011). "High-Frequency Turbulence and Suspended Sediment Concentration Measurements in the Garonne River Tidal Bore." *Estuarine Coastal and Shelf Science*, Vol. 95, No. 2-3, pp. 298-306 (DOI 10.1016/j.ecss.2011.09.012).

CHANSON, H., TAKEUCHI, M., and TREVETHAN, M. (2007). "High-Frequency Suspended Sediment Flux Measurements in a Small Estuary." *Proc. 6th International Conference on Multiphase Flow ICMF 2007*, Leipzig, Germany, July 9-13, M. SOMMERFIELD Editor, Session 7, Paper No. S7_Mon_C_S7_Mon_C_5, 12 pages (CD-ROM) (ISBN 978-3-86010-913-7).

CHANSON, H., and TREVETHAN, M. (2011). "Vertical Mixing in the Fully Developed Turbulent Layer of Sediment-Laden Open-Channel Flow. Discussion." *Journal of Hydraulic Engineering*, ASCE, Vol. 137, No. 9, pp. 1095-1097 (DOI: 10.1061/(ASCE)HY.1943-7900.0000218).

CHEN, Jiyu, LIU, Cangzi, ZHANG, Chongle, and WALKER, H.J. (1990). "Geomorphological Development and Sedimentation in Qiantang Estuary and Hangzhou Bay." *Jl of Coastal Res.*, Vol. 6, No. 3, pp. 559-572.

CHEN, S. (2003). "Tidal Bore in the North Branch of the Changjiang Estuary." *Proc. Intl Conf. on Estuaries & Coasts ICEC-2003*, Hangzhou, China, Nov. 8-11, Intl Research & Training Center on Erosion & Sedimentation Ed., Vol. 1, pp. 233-239.

DOCHERTY, N.J., and CHANSON, H. (2012). "Physical Modelling of Unsteady Turbulence in Breaking Tidal Bores." *Journal of Hydraulic Engineering*, ASCE, Vol. 138, No. 5, pp. 412-419 (DOI: 10.1061/(ASCE)HY.1943-7900.0000542).

FURUYAMA, S., and CHANSON, H. (2010). "A Numerical Solution of a Tidal Bore Flow." *Coastal Engineering Journal*, Vol. 52, No. 3, pp. 215-234 (DOI: 10.1142/S057856341000218X).

GRAF, W.H. (1971). "Hydraulics of Sediment Transport." *McGraw-Hill*, New York, USA.

GREB, S.F., and ARCHER, A.W. (2007). "Soft-Sediment Deformation Produced by Tides in a Meizoseismic Area, Turnagain Arm, Alaska." *Geology*, Vol. 35, No. 5, pp. 435-438.

HA, H.K., HSU, W.Y., MAA, J.P.Y., SHAO, Y.Y., and HOLLAND, C.W. (2009). "Using ADV Backscatter Strength

for Measuring Suspended Cohesive Sediment Concentration." *Continental Shelf Research*, Vol. 29, pp. 1310-1316.

HENDERSON, F.M. (1966). "Open Channel Flow." *MacMillan Company*, New York, USA.

HORNUNG, H.G., WILLERT, C., and TURNER, S. (1995). "The Flow Field Downstream of a Hydraulic Jump." *Jl of Fluid Mech.*, Vol. 287, pp. 299-316.

JULIEN, P.Y. (1995). "Erosion and Sedimentation." *Cambridge University Press*, Cambridge, UK, 280 pages.

KHEZRI, N., and CHANSON, H. (2012). "Inception of Bed Load Motion beneath a Bore." *Geomorphology*, Vol. 153-154, pp. 39-47 (DOI: 10.1016/j.geomorph.2012.02.006).

KJERFVE, B., and FERREIRA, H.O. (1993). "Tidal Bores: First Ever Measurements." *Ciência e Cultura (Jl of the Brazilian Assoc. for the Advancement of Science)*, Vol. 45, No. 2, March/April, pp. 135-138.

KOCH, C., and CHANSON, H. (2009). "Turbulence Measurements in Positive Surges and Bores." *Journal of Hydraulic Research*, IAHR, Vol. 47, No. 1, pp. 29-40 (DOI: 10.3826/jhr.2009.2954).

LIGHTHILL, J. (1978). "Waves in Fluids." *Cambridge University Press*, cambridge, UK, 504 pages.

LUBIN, P., GLOCKNER, S., and CHANSON, H. (2010). "Numerical Simulation of a Weak Breaking Tidal Bore." *Mechanics Research Communications*, Vol. 37, No. 1, pp. 119-121 (DOI: 10.1016/j.mechrescom.2009.09.008).

McLELLAND, S.J., and NICHOLAS, A.P. (2000). "A New Method for Evaluating Errors in High-Frequency ADV Measurements." *Hydrological Processes*, Vol. 14, pp. 351-366.

MOUAZE, D., CHANSON, H., and SIMON, B. (2010). "Field Measurements in the Tidal Bore of the Sélune River in the Bay of Mont Saint Michel (September 2010)." *Hydraulic Model Report No. CH81/10*, School of Civil Engineering, The University of Queensland, Brisbane, Australia, 72 pages (ISBN 9781742720210).

MOULE, A.C. (1923). "The Bore on the Ch'ien-T'ang River in China." *T'oung Pao*, Archives pour servir à l'étude de l'histoire, des langues, la geographie et l'ethnographie de l'Asie Orientale (Chine, Japon, Corée, Indo-Chine, Asie Centrale et Malaisie), Vol. 22, pp. 10-188.

OTSUBO, K. and MURAOKO, K. (1988). "Critical Shear Stress of Cohesive Bottom Sediments." *Journal of Hydraulic Engineering*, Vol. 114, No. 10, pp. 1241-1256.

REUNGOAT, D., CHANSON, H., and CAPLAIN, B. (2012). "Field Measurements in the Tidal Bore of the Garonne River at Arcins (June 2012)." *Hydraulic Model Report No. CH89/12*, School of Civil Engineering, The University of Queensland, Brisbane, Australia, 121 pages (ISBN 9781742720616).

ROUSSEL, N., LE ROY, R., and COUSSOT, P. (2004). "Thixotropy Modelling at Local and Macroscopic Scales." *Jl of Non-Newtonian Fluid Mech.*, Vol. 117, No. 2-3, pp. 85-95.

ROWBOTHAM, F. (1983). "The Severn Bore." *David & Charles*, Newton Abbot, UK, 3rd edition, 104 pages.

SIMPSON, J.H., FISHER, N.R., and WILES, P. (2004). "Reynolds Stress and TKE Production in an Estuary with a Tidal Bore." *Estuarine, Coastal and Shelf Science*, Vol. 60, No. 4, pp. 619-627.

TESSIER, B., and TERWINDT, J.H.J. (1994). "An Example of Soft-Sediment Deformations in an intertidal Environment - The Effect of a Tidal Bore". *Comptes-Rendus de l'Académie des Sciences*, Série II, Vol. 319, No. 2, Part 2, pp. 217-233 (in French).

TOORMAN, E.A. (2008). "Vertical Mixing in the Fully Developed Turbulent Layer of Sediment-Laden Open-Channel Flow." *Journal of Hydraulic Engineering*, ASCE, Vol. 134, No. 9, pp. 1225-1235 DOl: 10.1 061/(ASCE)0733-9429(2008) 134:9(1225).

TRICKER, R.A.R. (1965). "Bores, Breakers, Waves and Wakes." *American Elsevier Publ. Co.*, New York, USA.

WOLANSKI, E., WILLIAMS, D., SPAGNOL, S., and CHANSON, H. (2004). "Undular Tidal Bore Dynamics in the Daly Estuary, Northern Australia." *Estuarine, Coastal and Shelf Science*, Vol. 60, No. 4, pp. 629-636.

ZHANG, J.L., and LIU, D.X. (2011). "Application of OBS-3A Nephelometer in Observation of Tidal Bore in Qiantang River." *Ocean Technology*, Vol. 30, No. 2, pp. 67-79 (in Chinese).

ZHOU, X.J., and GAO, S. (2004). "Spatial Variability and Representation of Seabed Sediment Grain Sizes: an Example from the Zhoushan-Jinshanwei Transect, Hangzhou Bay, China." *Chinese Science Bulletin*, Vol. 49, No. 23, pp. 2503-2507.

Table 1 - Tidal bore field measurements in the Arcins channel, Garonne River (France)

Ref. (1)	Date (2)	Tidal range (m) (3)	ADV system (4)	Sampling rate (Hz) (5)	Sampling duration (6)	Start time (7)	Tidal bore time (8)	End time (9)	ADV sampling volume (10)	Bore type (11)	Fr_1 (12)	U (13)	d_1 (14)	A_1 (15)	A_2/A_1 (16)
CHANSON et al. (2011)	10/09/2010	6.03	Nortek Vector (6MHz)	64	2h 45 min	17:15	18:17	20:00	About 7 m from right bank waterline (at low tide), 0.81 m below water surface.	Undular	1.30	4.49	1.77	105.7	1.37
	11/09/2010	5.89	Nortek Vector (6MHz)	64	2h 20 min	18:00	18:59	20:10	About 7 m from right bank waterline (at low tide), 0.81 m below water surface.	Undular	1.20	4.20	1.81	108.8	1.33
Present study	7/06/2012	5.68	Sontek microADV (50 Hz)	50	2h 58 min (10,694 s)	06:01	06:44	09:00	About 11.58 m from right bank waterline (at low tide), 1.03 m below water surface.	Undular	1.02	3.85	2.72	158.9	1.23
		5.5	Visual observations	N/A	N/A	N/A	18:47	N/A	N/A.	Undular	1.19	4.58	2.65	152.3	1.28

Notes: A_1: channel cross-section area immediately prior to the bore passage; A_2: channel cross-section area immediately after the bore passage; d_1: water depth next to ADV immediately prior to the bore passage; Fr_1: tidal bore Froude number (Eq. (1)); U: tidal bore celerity positive upstream on the channel centreline; Tidal range: measured at Bordeaux; All times are in French local times.

Table 2 - Unusual observations of delays between tidal bore passage and flow reversal (Field observations)

Reference	River	Date	Location	Flow reversal delay	Remarks
(1)	(2)	(3)	(4)	(5)	(6)
PARTIOT in BAZIN (1865)	Seine (France)	13/09/1855	Chapel Barre-y-Va		Undular bore
			Next to surface	+130 s	
			3.3 m below surface	+90 s	
		25/09/1855	Vallon de Caudebecquet, Next to surface	+145 s	Undular bore
			1.5 m below surface	+60 s	
			next to bottom	+60 s	
KJERFVE and FERREIRA (1993)	Rio Mearim (Brazil)	30/01/1991	Location D, 0.7 m above bottom	-60 s	Undular bore
Present study	Garonne (France)	7/06/2012 morning	Arcins, Surface data	+6 s	Undular (Fr_1 = 1.02)
			1.03 m below surface	+50 s	

Note: Flow reversal delay positive when the longitudinal velocity direction changed after the bore front passage.

Table 5-3 - Integral time scales in terms longitudinal velocity V_x, suspended sediment concentration SSC and sediment flux q_s data before and after the tidal bore of the Garonne River on 7 June 2012 morning

Flow parameter	Statistical property	Before bore 23,130 < t < 24,130 s	After bore 24,250< t < 25,250 s	Units
V_x	Mean	0.394	-0.548	m/s
	T_{Vx}	2.4	52	s
SSC	Mean	34.3	31.3	kg/m^3
	T_{SSC}	0.22	8.0	s
q_s	Mean	13.51	-17.15	$kg/m^2/s$
	T_{qs}	2.6	52	s

Notes: Before bore: 23,130 < t < 24,130 s; After bore: 24,250< t < 25,250 s; T: auto-correlation time scale.

FIGURE CAPTIONS

Fig. 1 - Photographs of the undular tidal bore of the Garonne River in the Arcins channel

(A) Looking downstream at the incoming undular tidal bore in the Arcins channel on 5 June 2012 at 17:33:54

(B) Tidal bore approaching the pontoon on 7 June 2012 at 06:51:41 - The red arrow points to the bore front

(C) Undular bore passing the sampling point on 7 June 2012 at 18:54:52 - Bore propagation from right to left with the kayak tried to surf the bore front

Fig. 2 - Garonne River near Arcins

(A) Map of the river channel (inset: Map of France)

(B) Sketch of the tidal bore of the Garonne River main channel entering into the southern end of the Arcins channel and propagating northwards against the flood flow in the Arcins channel

Fig. 3 - Arcins channel cross-section and observed water levels

(A) Surveyed cross-section of Arcins channel looking upstream with the low tide water level on 7 June 2012 afternoon and the corresponding ADV sampling volume location - Comparison between the 2010 and 2012 surveys at the same cross-section

(B) Un-distorted sketch of the ADV mounting, sampling volume location and water surface 20 minutes prior to the tidal bore on 7 June 2012 morning- Left: view from Arcins Island - Right: looking upstream

(C) Measured water elevations in the Arcins channel on 7 June 2012 and in Bordeaux (44°52'N, 0°33'W) (Data: Vigicrue, Ministère de l'Environnement et du Développement Durable)

Fig. 4 - Time-variations of the water depth, free-surface velocity, water temperature, salinity, longitudinal and transverse velocity component (ADV data), suspended sediment concentration, and longitudinal sediment flux on 7 June 2012 morning in Arcins about the tidal bore passage

(A) Water depth next to the ADV unit

(B) Water temperature and salinity

(C) Longitudinal and transverse velocity component (ADV data)

(D) Suspended sediment concentration estimate and longitudinal suspended sediment flux

Fig. 5 - Time-variations of the water depth, free-surface velocity, water temperature and salinity on 7 June 2012 afternoon in Arcins about the tidal bore passage

(A) Water depth next to the ADV unit

(B) Water temperature and salinity

Fig. 6 - Details of the time variations of the water depth and turbulent velocity components in the tidal bore of the Garonne River on 7 June 2012

Fig. 7 - Loading and unloading cycle with a rheometer Malvern Kinexus Pro equipped with a smooth cone (40 mm, 4º) - Sediment collection: 7 June 2012 at low tide and 8 June 2012 at mid-ebb tide

Fig. 8 - Relationship between suspended sediment concentration and acoustic signal amplitude with the sediment samples collected at Arcins - Comparison between the data and Equations (3) and (4)

Fig. 9 - Suspended sediment flux q_s ($kg.s^{-1}.m^{-2}$) as function of the suspended sediment concentration SSC - Comparison between present data (Garonne 2012), the 2010 observations (Garonne 2010) together with observations in estuaries (Eprapah) and rivers during floods (Amazon, Brisbane, Fitzroy, Huanghe, Mississippi, Nile, North Fork Toutle, Rio Puerco)

Fig. 1 - Photographs of the undular tidal bore of the Garonne River in the Arcins channel

(A) Looking downstream at the incoming undular tidal bore in the Arcins channel on 5 June 2012 at 17:33:54

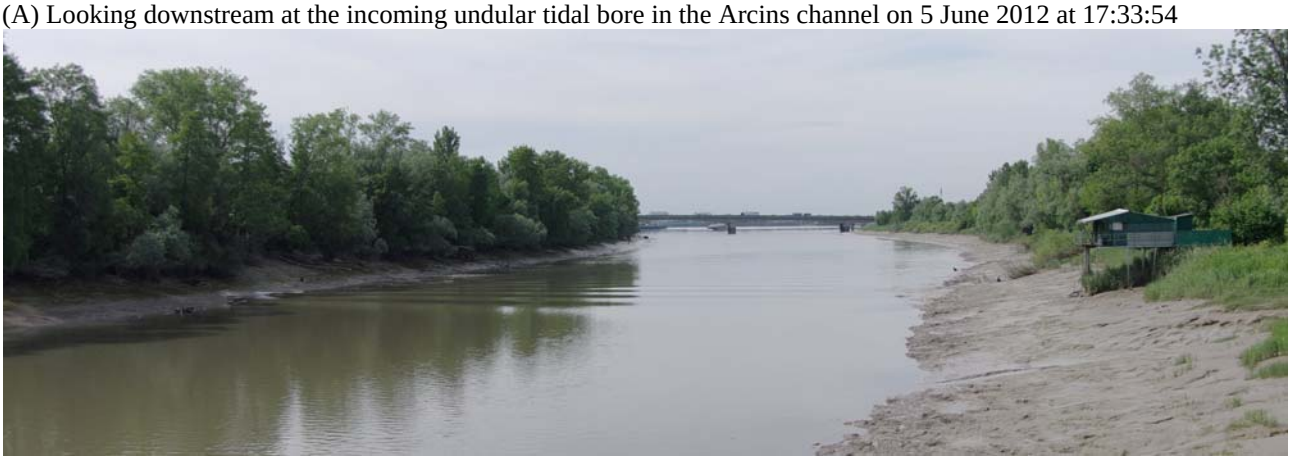

(B) Tidal bore approaching the pontoon on 7 June 2012 at 06:51:41 - The red arrow points to the bore front

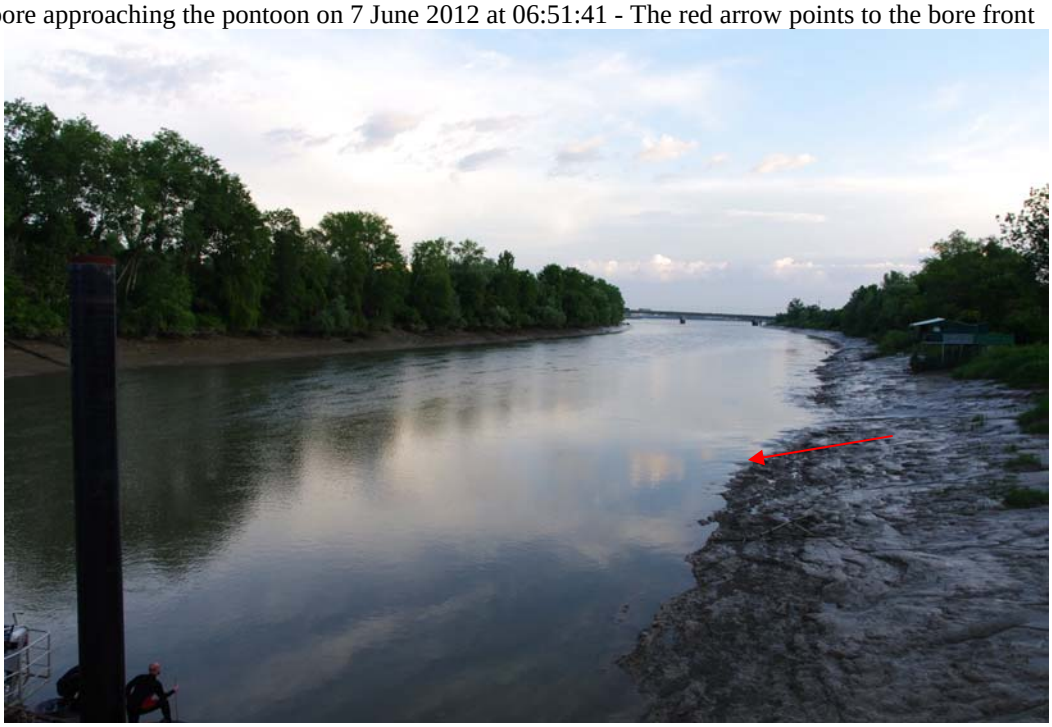

(C) Undular bore passing the sampling point on 7 June 2012 at 18:54:52 - Bore propagation from right to left with the kayak tried to surf the bore front

Fig. 2 - Garonne River near Arcins

(A) Map of the river channel (inset: Map of France)

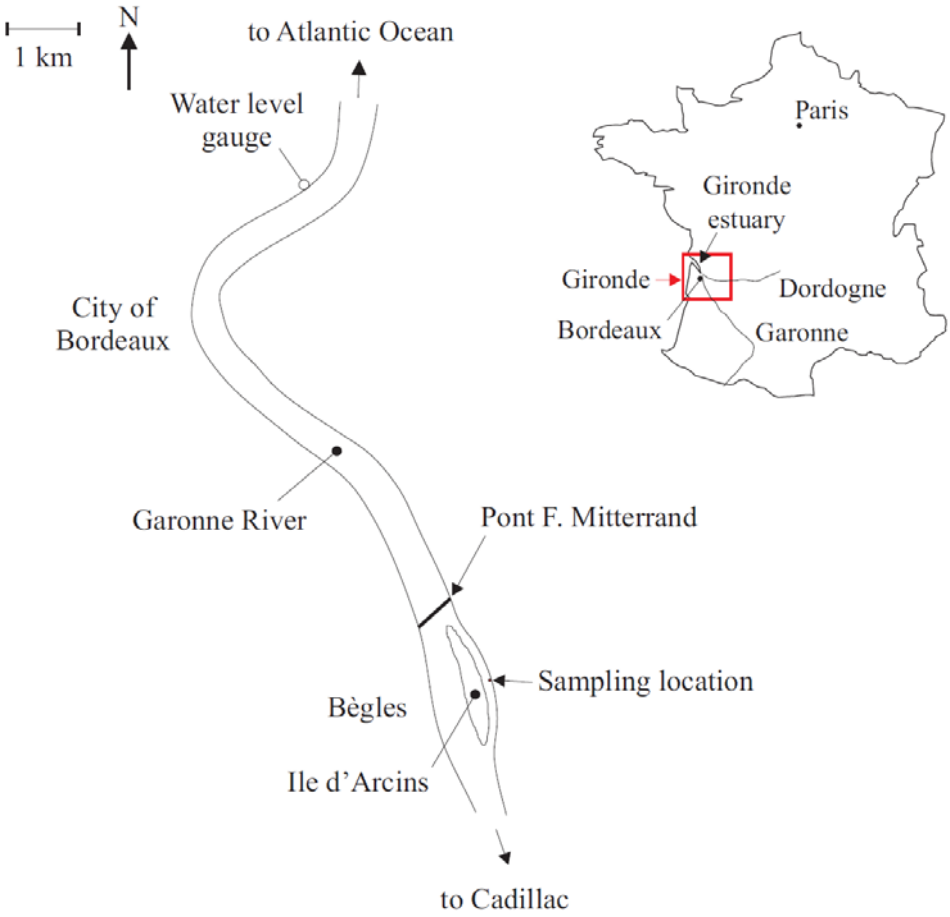

(B) Sketch of the tidal bore of the Garonne River main channel entering into the southern end of the Arcins channel and propagating northwards against the flood flow in the Arcins channel

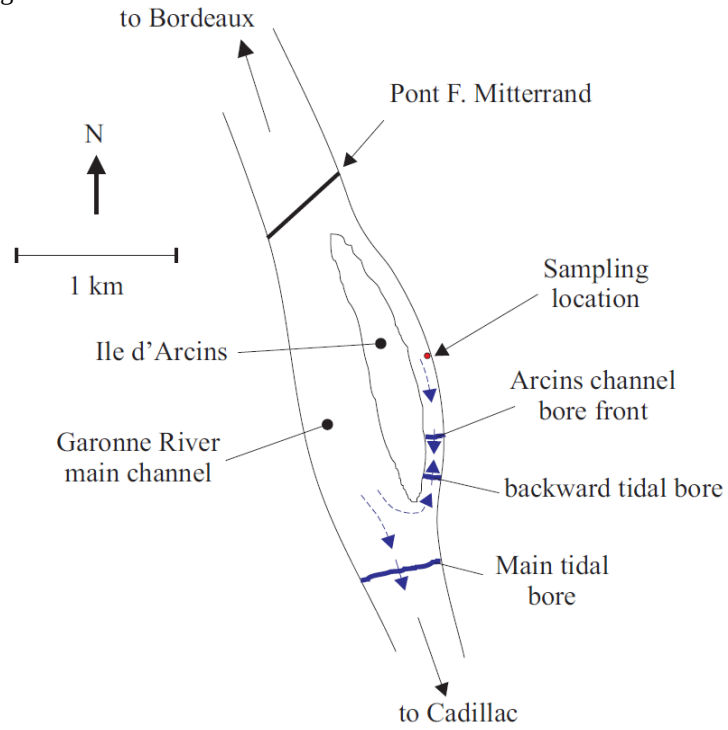

Fig. 3 - Arcins channel cross-section and observed water levels

(A) Surveyed cross-section of Arcins channel looking upstream with the low tide water level on 7 June 2012 afternoon and the corresponding ADV sampling volume location - Comparison between the 2010 and 2012 surveys at the same cross-section

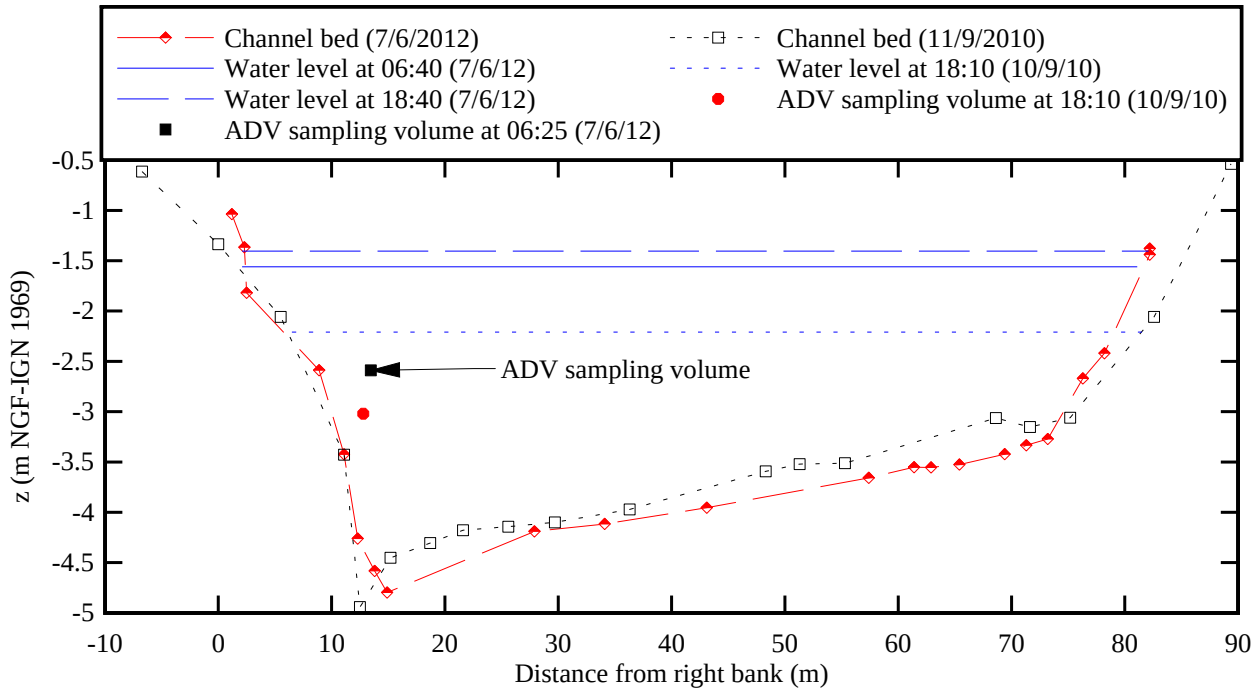

(B) Un-distorted sketch of the ADV mounting, sampling volume location and water surface 20 minutes prior to the tidal bore on 7 June 2012 morning- Left: view from Arcins Island - Right: looking upstream

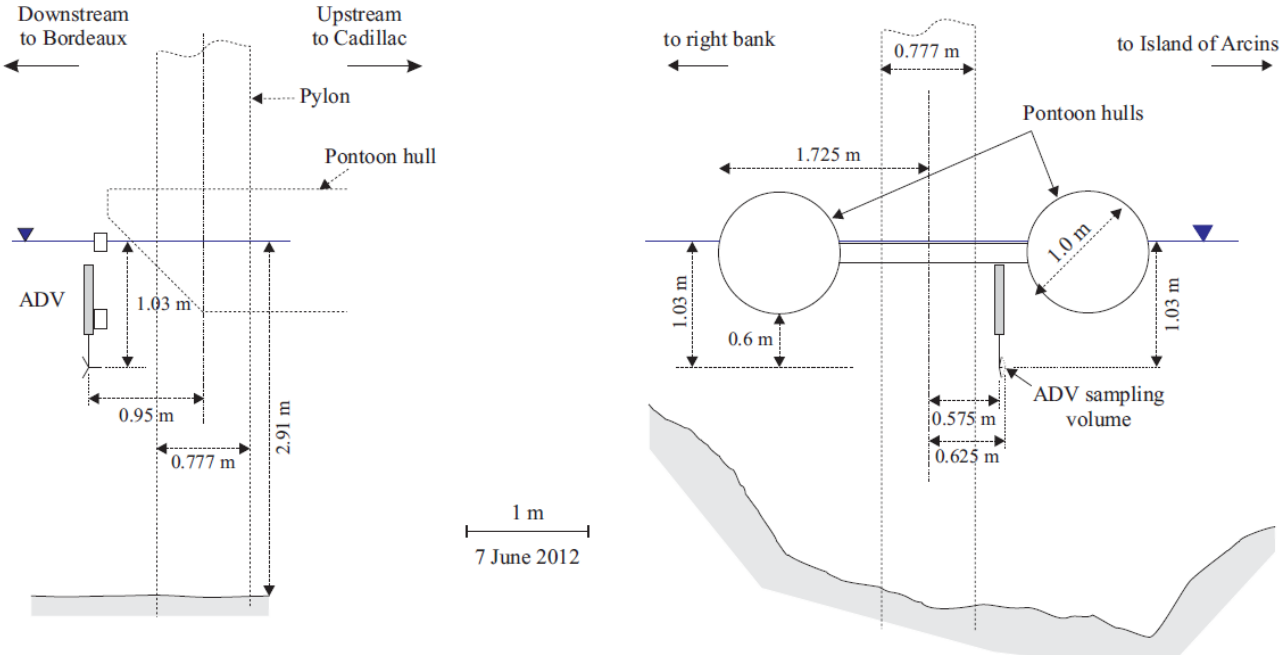

(C) Measured water elevations in the Arcins channel on 7 June 2012 and in Bordeaux (44°52'N, 0°33'W) (Data: Vigicrue, Ministère de l'Environnement et du Développement Durable)

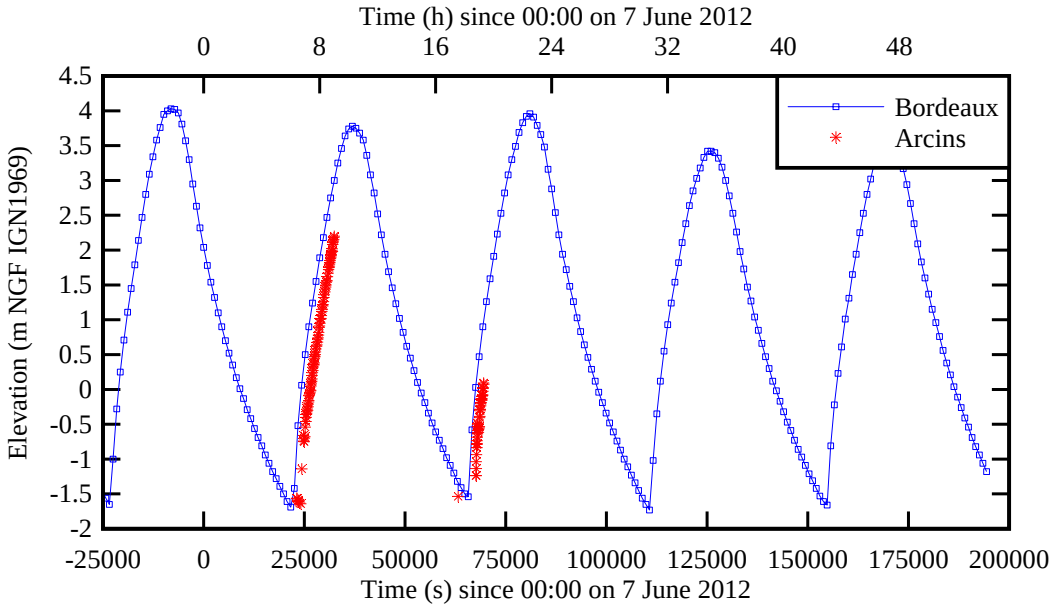

Fig. 4 - Time-variations of the water depth, free-surface velocity, water temperature, salinity, longitudinal and transverse velocity component (ADV data), suspended sediment concentration, and longitudinal sediment flux on 7 June 2012 morning in Arcins about the tidal bore passage

(A) Water depth next to the ADV unit

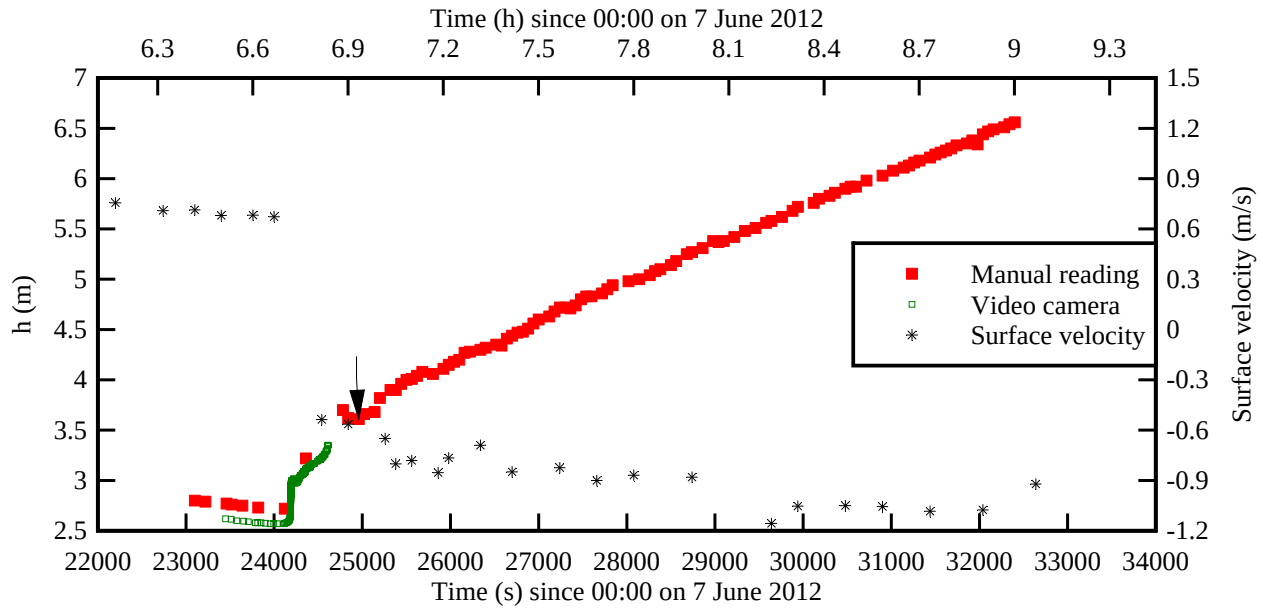

(B) Water temperature and salinity

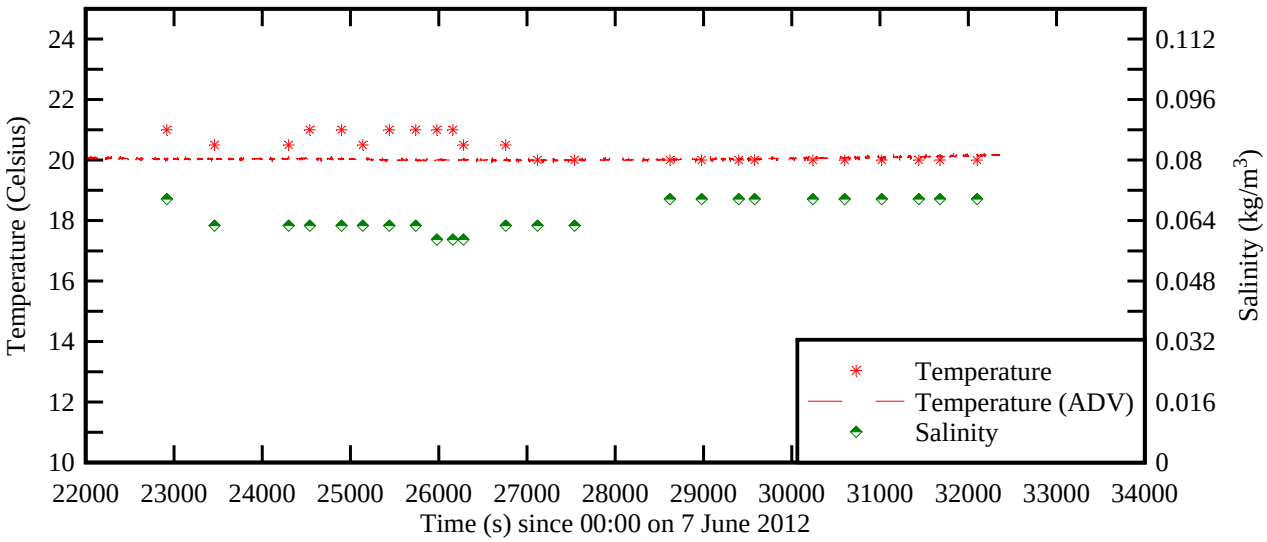

(C) Longitudinal and transverse velocity component (ADV data)

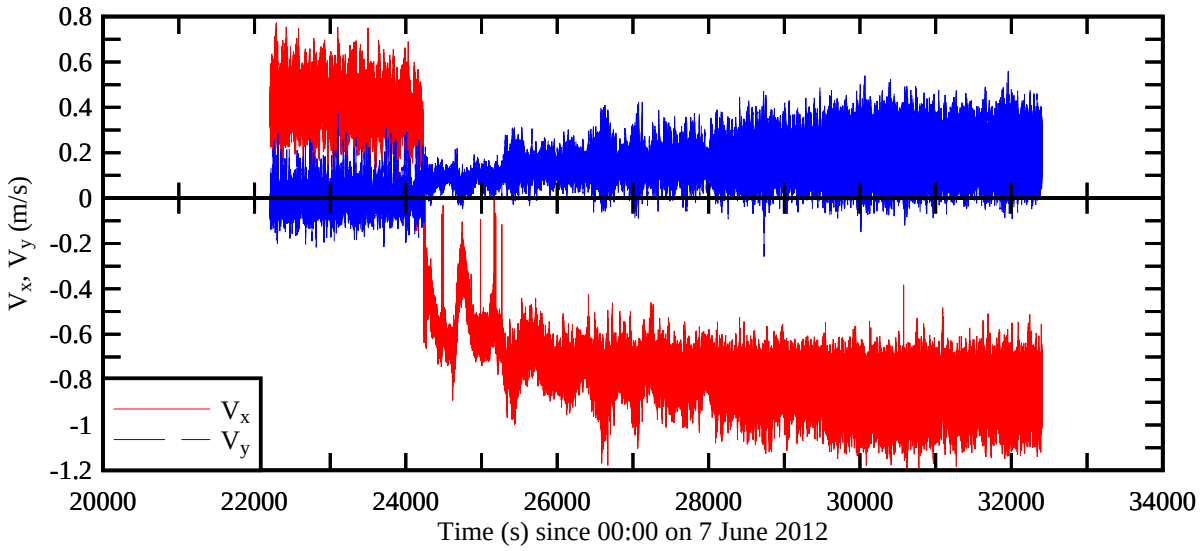

(D) Suspended sediment concentration estimate and longitudinal suspended sediment flux

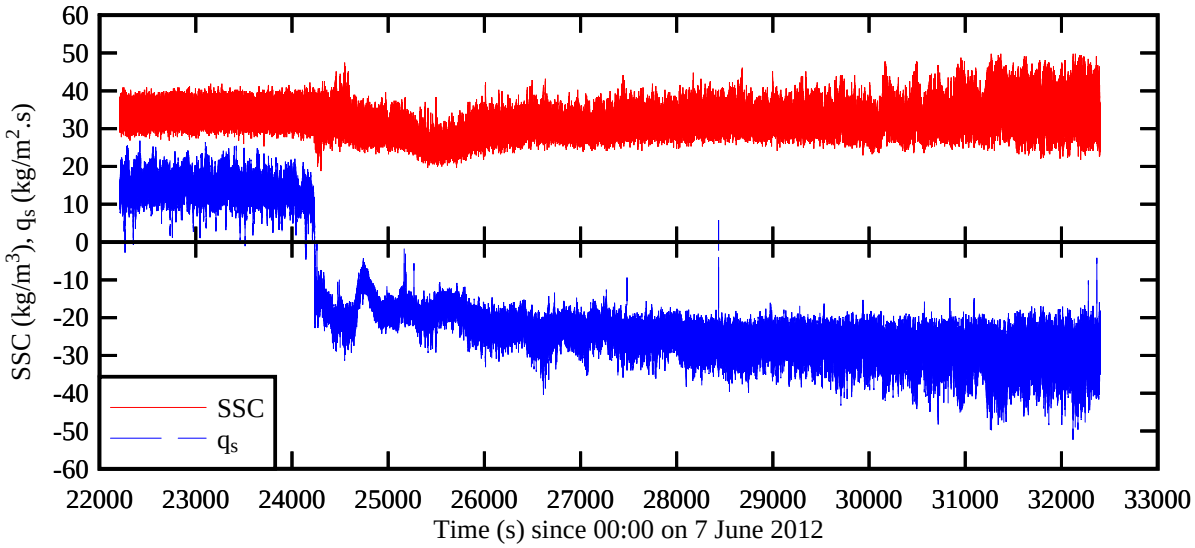

Fig. 5 - Time-variations of the water depth, free-surface velocity, water temperature and salinity on 7 June 2012 afternoon in Arcins about the tidal bore passage

(A) Water depth next to the ADV unit

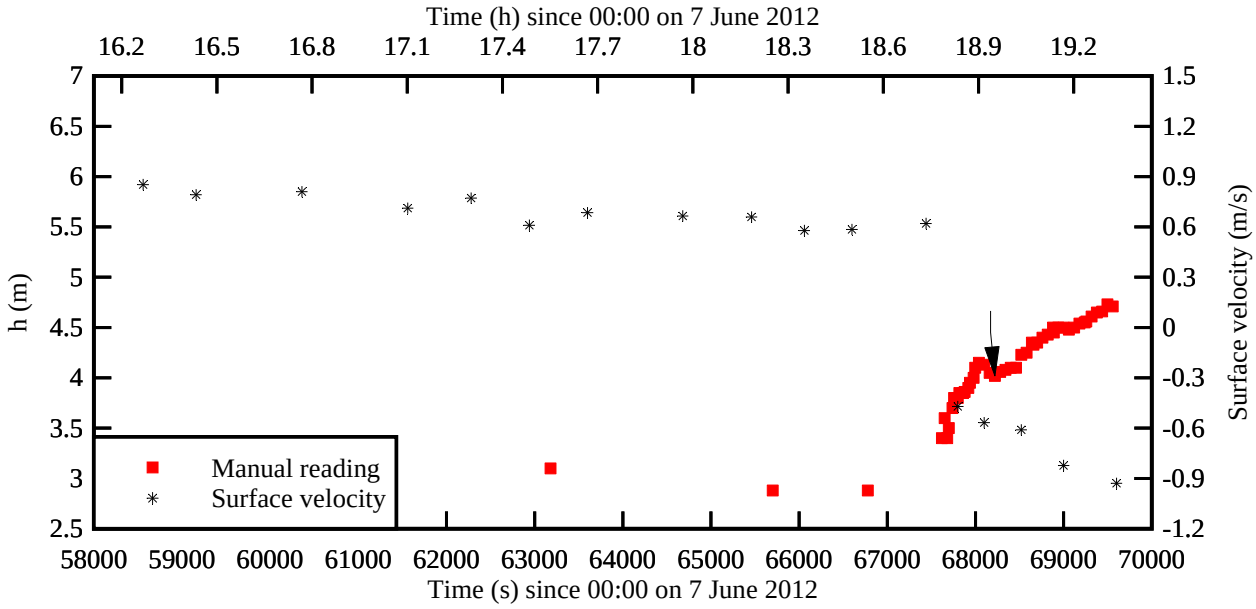

(B) Water temperature and salinity

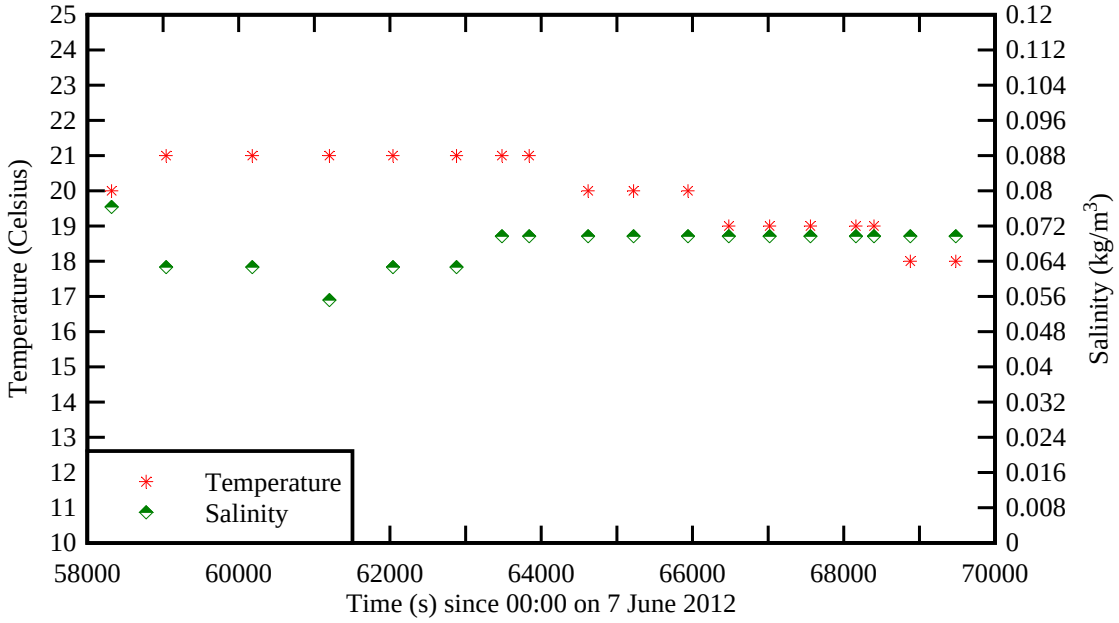

Fig. 6 - Details of the time variations of the water depth and turbulent velocity components in the tidal bore of the Garonne River on 7 June 2012

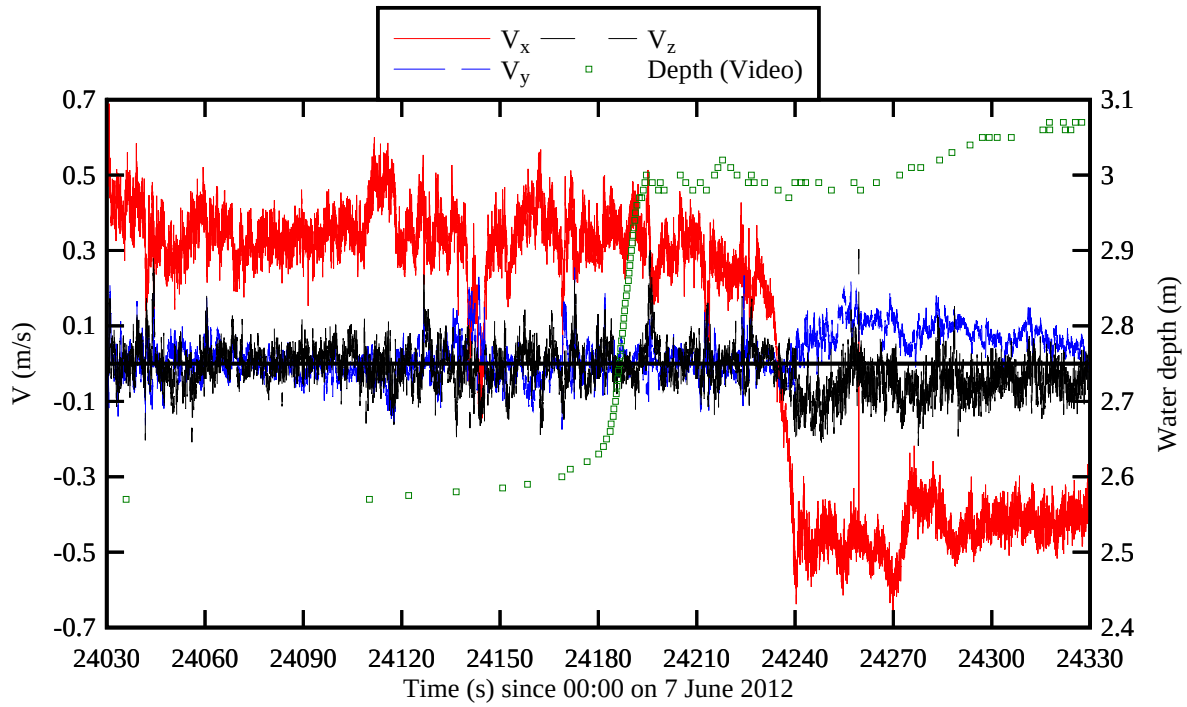

Fig. 7 - Loading and unloading cycle with a rheometer Malvern Kinexus Pro equipped with a smooth cone (40 mm, 4º)

- Sediment collection: 7 June 2012 at low tide and 8 June 2012 at mid-ebb tide

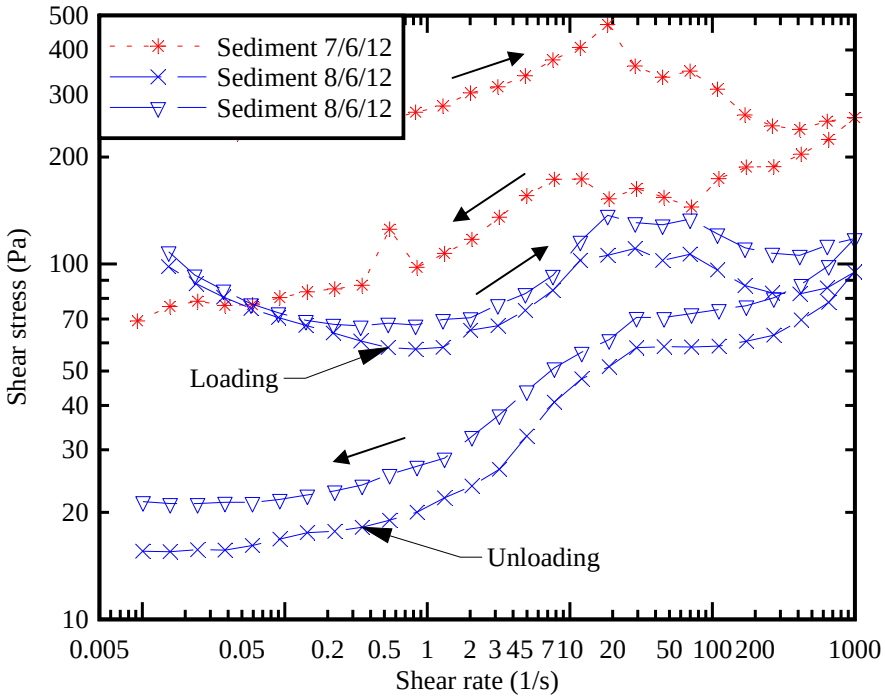

Fig. 8 - Relationship between suspended sediment concentration and acoustic signal amplitude with the sediment samples collected at Arcins - Comparison between the data and Equations (3) and (4)

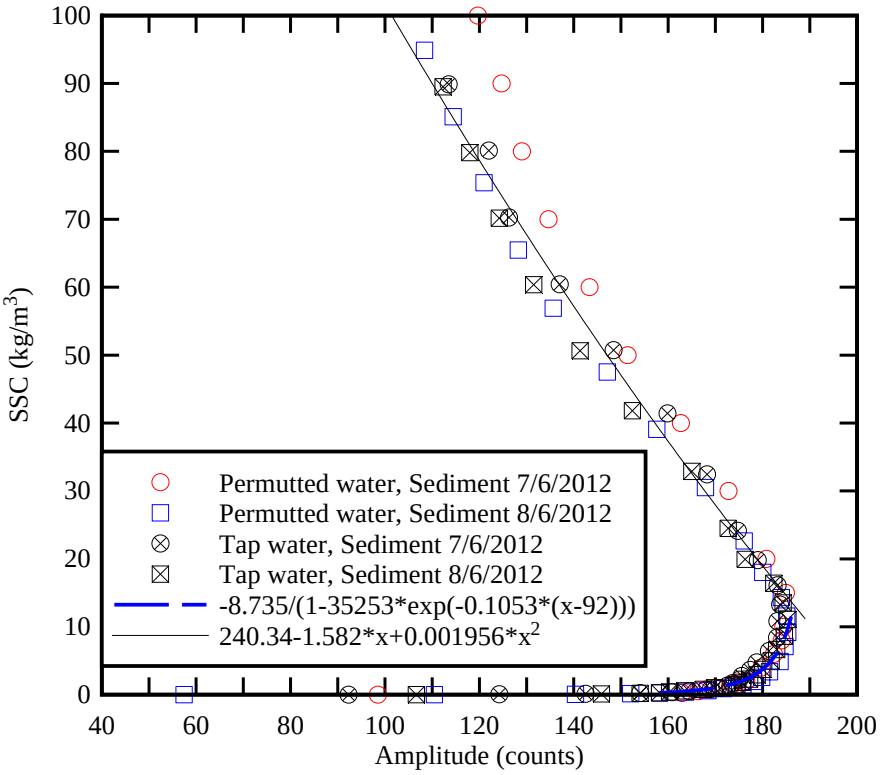

Fig. 9 - Suspended sediment flux q_s ($kg.s^{-1}.m^{-2}$) as function of the suspended sediment concentration SSC - Comparison between present data (Garonne 2012), the 2010 observations (Garonne 2010) together with observations in estuaries (Eprapah) and rivers during floods (Amazon, Brisbane, Fitzroy, Huanghe, Mississippi, Nile, North Fork Toutle, Rio Puerco)